Runsheng Xu*, Wei Wang*, Weilin Chen, Bin Jia and Zhihui Xu

3D Microstructure and Micromechanical Properties of Minerals in Vanadium-Titanium Sinter

https://doi.org/10.1515/htmp-2017-0181
Received December 07, 2017; accepted May 22, 2018

Abstract: To investigate the structural characteristics and mechanical properties of minerals in vanadium-titanium sinter, the 3D microstructures of the sinter were reconstructed by serial sectioning in conjunction with computer-aided 3D reconstruction techniques The results show that hematite and magnetite in vanadium-titanium sinter will grow along the longitudinal axis direction and act as a scaffold. The size of magnetite crystals in vanadium-titanium sinter is much smaller than that in traditional sinter. The calcium ferrite in vanadium-titanium sinter is columnar-like, while that in traditional sinter is needle-like. The decreasing order of the microhardness value of minerals in the two sinters is hematite, calcium ferrite, magnetite and silicate, while the fracture toughness value from highest to lowest is calcium ferrite, hematite, magnetite and silicate. The comprehensive hardness value and comprehensive fracture toughness value of vanadium-titanium sinter are both less than these of traditional sinter.

Keywords: vanadium-titanium sinter, 3D microstructure, microhardness, fracture toughness, mineral

Introduction

Iron ore sinter is one of the most important raw materials for blast furnace ironmaking. The quality improvement of sinter not only contributes to the operational stability of the blast furnace but also increases the hot metal yield as well as the economic benefits [1, 2]. A previous study revealed that the sinter quality depended on the microstructure and micromechanical properties of the minerals in sinter [3]. However, numerous reports have focused on the minerals in traditional sinter, and the features of minerals in vanadium-titanium sinter were rarely investigated. Moreover, reported studies on the characterization of minerals are based on two-dimensional (2D) images taken by polarizing optical microscopy or scanning electron microscopy. Fan et al. developed a system to analyze the mineral components of sinter accurately and rapidly based on the features of mineralogy micrographs of sinter [4]. Lv et al. investigated the relationship between the mineragraphical features of iron-ore sinter and its gray histogram [5], and the gray-level co-occurrence matrix was used as an effective method to examine the texture features of the main minerals in sinter [6]. However, the mineral structure in sinter is rather complicated, and a 2D image cannot adequate display its complicated three-dimensional (3D) features. Therefore, the microstructure of the mineral cannot be obtained directly and accurately using a 2D image. With the progress of computer science and technology, visualization technology based on 3D reconstruction has been greatly developed. Thus, some studies were conducted to analyze the 3D pore structure of the sinter using X-ray CT technology [7–10]. However, these studies could not reveal the 3D structures of different minerals in sinter.

The microscopic mechanical properties of minerals in traditional sinter have been investigated by many scholars at home and abroad. Wang et al. [11, 12] detected the microhardness of minerals in sinter, showing that the value of microhardness from high to low was hematite, calcium ferrite, magnetite and silicate. Sakamoto et al. [13] performed some studies on the crack initiation behaviors of minerals using the Vickers indentation method and concluded that the crack characteristics varied among different minerals. Using the same method, Ying and Shigaki et al. [14, 15] investigated the fracture toughness of calcium ferrites in different crystal structures. Furthermore, Loo et al. [16] defined the comprehensive fracture toughness and investigated the relationship between the reduction degradation indices of sinter and its comprehensive fracture toughness. However, the above studies mostly focused on traditional sinter, and reports on the micromechanical properties of minerals in vanadium-titanium sinter were

***Corresponding authors: Runsheng Xu:**
E-mail: xu_runsheng@163.com, **Wei Wang:**
E-mail: wangwei74@wust.edu.cn, State Key Laboratory of Refractories and Metallurgy, Wuhan University of Science and Technology, Wuhan 430081, China; Key Laboratory for Ferrous Metallurgy and Resources Utilization of Ministry of Education, Wuhan University of Science and Technology, Wuhan 430081, China
Weilin Chen, Bin Jia, Zhihui Xu, Ironmaking Plant, Wuhan Iron and Steel Co., Ltd., Wuhan 430083, China

limited. In fact, in China, particularly in the Panzhihua region, various vanadium-titanium sinters were used in blast furnaces. The practice showed that the quality of vanadium-titanium sinter was lower than traditional sinter, which contributed to the deterioration of the operational condition of the blast furnace. Therefore, it is essential to conduct the further research on vanadium-titanium magnetite sinter. The present work aims to study the influence factors of the metallurgical properties of vanadium-titanium sinter based on the microstructures and micromechanical properties of minerals. First, the 3D microstructures of the minerals in sinter were reconstructed using serial sectioning and 3D reconstruction technology [17–20]. Second, the microhardness and fracture toughness of different minerals were tested by a Vickers hardness tester [21]. Furthermore, the difference in the 3D microstructures and micromechanical properties of minerals between vanadium-titanium sinter and traditional sinter were investigated in detail in this study. The present research results, therefore, are important for increasing the understanding of the inherent properties of vanadium-titanium magnetite sinter and can provide a significant foundation for the optimization of the sinter quality.

Materials and methods

Materials

The sinter samples were obtained from two ironmaking plants. One sinter was manufactured from vanadium-titanium magnetite ore, and the other used hematite ore as the raw material for sintering. The chemical compositions of the sinters were tested using the X-ray fluorescence method. The reduction index (*RI*), tumbler index (*TI*) and reduction degradation index ($RDI_{-3.15}$) were measured according to the Chinese standards GB/T 13241-91, GB 8209-87 and GBI/T 13242-91, respectively. The chemical compositions and metallurgical properties of the two sinters were tested and are listed in Tables 1 and 2.

It can be found from Table 1 that vanadium-titanium sinter has more gangue minerals than traditional sinter, but the FeO content in the two sinters is similar. From Table 2, it can be observed that the vanadium-titanium sinter has a lower reduction index (*RI*), less tumbler index (*TI*), and greater reduction degradation index ($RDI_{-3.15}$) compared to the traditional sinter, which indicates that the metallurgical properties of traditional sinter are much better than those of the vanadium-titanium sinter.

Table 1: Chemical compositions of the sinters (mass %).

Sample	TFe	FeO	CaO	SiO_2	Al_2O_3	MgO	TiO_2	V_2O_5
Vanadium-titanium sinter	49.53	8.13	10.57	6.01	3.25	2.35	7.38	0.35
Traditional sinter	56.78	8.51	9.95	5.16	1.78	1.79	-	-

Table 2: Metallurgical properties of the sinters (%).

Sample	RI	$RDI_{-3.15}$	TI
Vanadium-titanium sinter	82.61	62.46	68.19
Traditional sinter	87.56	34.15	79.25

Reconstruction method of 3D sinter images

The 3D images of iron-ore sinters were obtained using serial sectioning and 3D reconstruction method, following the steps in Figure 1.

(1) The sinter samples were cut and then fixed to glass plates. After grinding and polishing, 2D microscopic images of samples were observed under an optical microscope at a magnification of 200X.
(2) The representative regions of the minerals were chosen for the microscopic images using an optical microscope. Selection of these regions of interest was very important but somewhat subjective. It was desirable to obtain several sections that encompassed various mineral partials in a given volume to allow entire particles to be reconstructed. In this study, three regions of each sinter were selected as the typical observation areas, and then nine pictures at each region were taken. The size of each image is approximately 1280×960 pixels.
(3) These pictures were introduced to a computer and stitched together by 3D Slicer software. Different minerals in the images were segmented and marked with different colors.
(4) Cyclic polishing and imaging of the sample surface were conducted to generate a series of microstructure sections. The thickness loss was approximately 2.5 μm per cycle, and 80 layers were completed in this study.

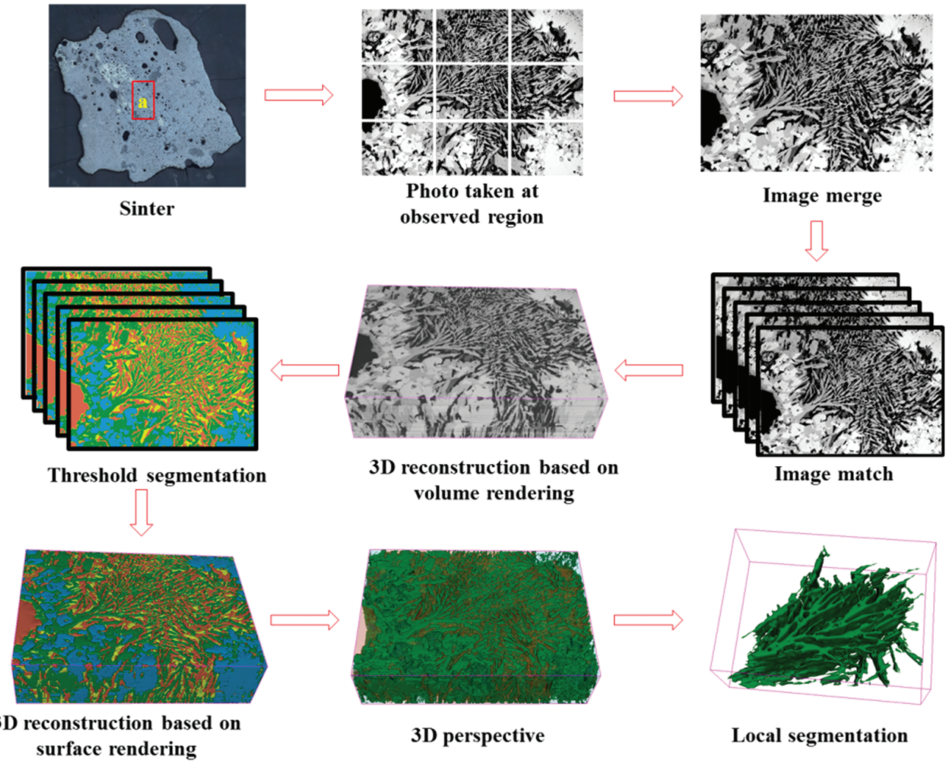

Figure 1: Flow chart of serial sectioning and 3D reconstruction process.

(5) The serial images of different sections were stacked, and the 3D morphologies of different minerals were reconstructed using the 3D Slicer software. In this work, the 3D reconstruction technology is based on the volume rendering method. The spatial distribution and perspectives of each mineral could be obtained through image segmentation technology.

(6) Because the structure of iron-ore sinter is rather complex, it is difficult to accurately segment the minerals in iron-ore sinter by the threshold method or other automatic segmentation methods. In this work, the method of human-computer interaction was used to segment and label the 3D images.

Test method of micromechanical properties of sinter

Mineral indentation was conducted by a Vickers hardness tester (HV-1000B). The loading parameter is important for this type of experiment. If the loading stress is too low, the crack of the mineral is not easily generated. In contrast, if the loading stress is too high, the mineral may be pulverized. Therefore, in this work, 300 g stress was designed for loading on the special mineral for 10 s. The hardness of each mineral was tested five times. The elastic modulus and fracture toughness of the minerals in sinter were calculated based on the follow equations [21–23]:

$$E = 0.45H/(1-n)\ (\mathrm{GN/m^2}) \tag{1}$$

$$K_{IC} = \delta\left(\frac{E}{H}\right)^{1/2}\cdot\frac{P}{c^{3/2}}\ (\mathrm{MN/m^{3/2}}) \tag{2}$$

where H is the microhardness, $\mathrm{GN/m^2}$; n is the ratio of the length of the short diagonal of indentation to the long diagonal; δ is 0.0153; E is elastic modulus, $\mathrm{GN/m^2}$; P is the loading stress, g; c is the average length of indentation crack diagonal, m; and K_{IC} is the fracture toughness, $\mathrm{MN/m^{3/2}}$.

Results and discussion

Distribution characteristic of minerals in the 3D image

Previous studies have shown that the main minerals in sinter are hematite, magnetite, calcium ferrite and silicate [4, 7, 11]. Beyond these, vanadium-titanium sinter had a few

perovskites [24]. To compare the 2D and 3D morphology of the minerals in sinter, three regions of each sinter were selected for investigation. The 2D image and 3D image of each selected region in the two sinters are shown in Figures 2 and 3. Since perovskite, the glass phase, sulfide and custerite were limited in sinter, these minerals were placed in the same category as silicate in this study. In the 3D image, the off-white part, blue part, green part, yellow part, and the orange-red part is hematite, magnetite, calcium ferrite, silicate and pore, respectively.

It can be observed from Figure 2 (the 2D image) that the majority of hematite in vanadium-titanium sinter presents as a euhedral crystal and coexists with magnetite. The magnetite in region (b) is anhedral crystals, mainly in the small granular form. In contrast, the magnetite in region (c) is euhedral crystals and coexists with hematite and calcium ferrite. More information can be found about the minerals from the 3D image. The primary minerals in vanadium-titanium sinter are hematite and magnetite, with sizes larger than those of other minerals. Along the longitudinal axis direction, hematite and magnetite crystals will continue to grow, and they act as a scaffold in the sinter. Some other small minerals, such as calcium ferrite and silicate, are wrapped by hematite or magnetite. It is interesting to note that unevenly distributed pores exist in the minerals. The 3D mineral structure of vanadium-titanium sinter indicates that the structural features of hematite and magnetite may be the important factors that affect the tumbler strength of the sinter due to its support role.

The mineral structure in traditional sinter is quite different from that in vanadium-titanium sinter, as shown in Figure 3. Acicular calcium ferrite interweaves with a small amount of silicate, and magnetite exists in a plate-shaped form in the 2D image of region (a). The 2D

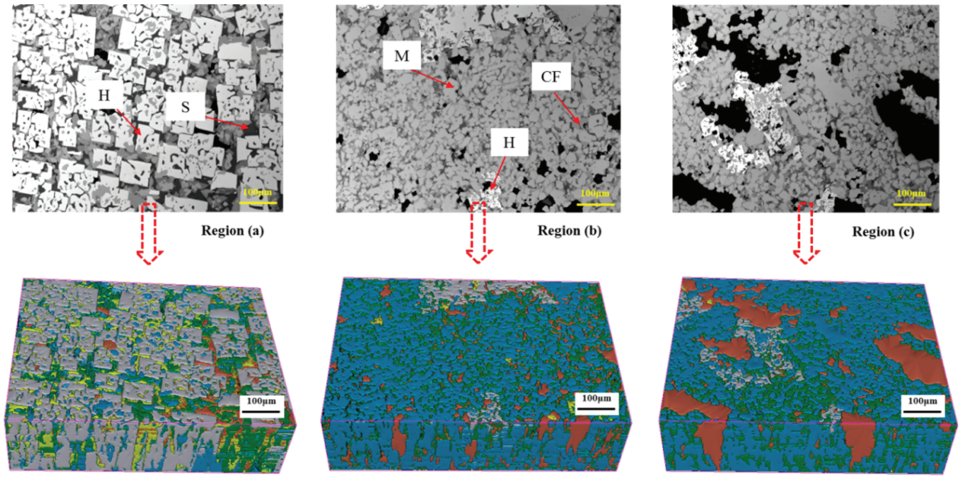

Figure 2: 2D and 3D images of selected regions in vanadium-titanium sinter.

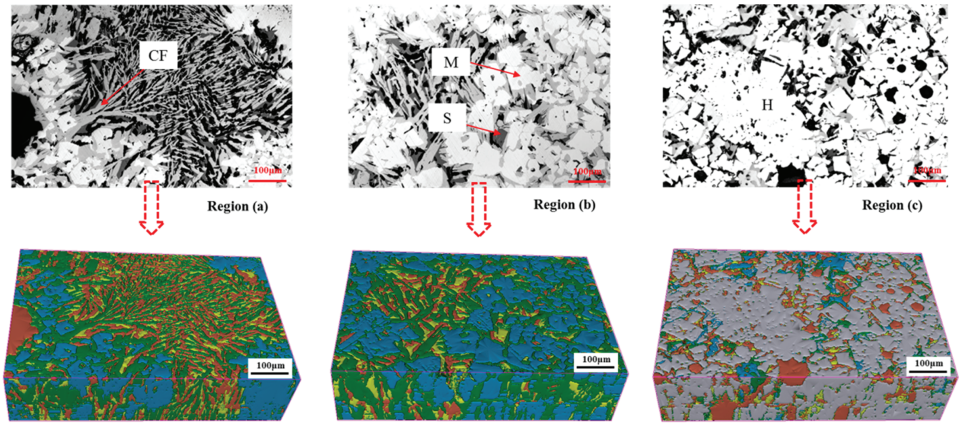

Figure 3: 2D and 3D images of selected regions in traditional sinter.

images of region (b) and region (c) are the aggregated areas of magnetite and hematite in traditional sinter, respectively. It can be observed that magnetite and hematite are flake-like, and their sizes are much larger than those of calcium ferrite and silicate. From the 3D image, the sizes of the minerals along the longitudinal axis direction are similar with that along the cross-sectional direction, indicating that the growth of the mineral has no direction. Though single calcium ferrite crystals are needle-like or columnar-like, they interweave with themselves or other small mineral particles, such as silicate, to form a big calcium ferrite group that contains many small pores. The calcium ferrite bridges the whole sinter volume in different directions and acts as an important matrix in the sinter. Therefore, the importance of calcium ferrite for determining the sinter quality in traditional sinter is confirmed through the analysis of the 3D distribution and mineral morphology.

3D microstructure of a single mineral

To better understand the characteristics of the 3D microstructure of the minerals in vanadium-titanium sinter and traditional sinter. The single mineral was segmented from the 3D reconstructed image, as shown in Figures 4, 5 and 6.

The 3D microstructure of hematite in vanadium-titanium sinter and traditional sinter is shown in Figure 4. It can be found that the 3D morphologies of hematite in the two sinters are quite different. The hematite in vanadium-titanium sinter exists as a scaffold shape or diamond shape, as shown in Figure 4 **(a) and (b)**. Its crystals connect with each other in the horizontal direction (Z axis). Furthermore, the size of the hematite grain gradually reduces as the sectioning layer increases, and some small hematite even disappears but still retaining the scaffold shape. The formation of this crystal type is mainly due to the weak crystallization ability caused by the fast cooling speed, which leads to the insufficient development of hematite crystals. This structural feature of hematite in the vanadium-titanium sinter easily results in the concentration of stress and the generation of cracks under stress loading. However, the morphology of hematite in traditional sinter is more irregular than that in vanadium-titanium sinter, as shown in Figure 4 **(c) and (d)**. There are many small pores and fine grains in the hematite structure, which easily form a melting corrosion structure with other minerals. This

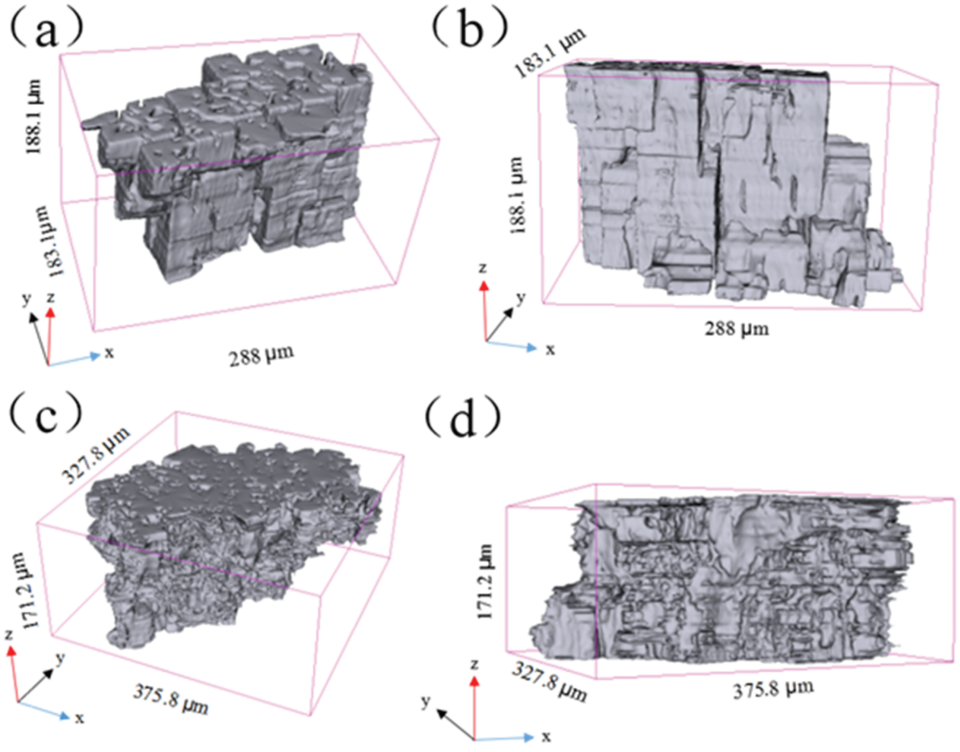

Figure 4: 3D microstructure of hematite in vanadium-titanium sinter (a), (b) and in traditional sinter (c), (d).

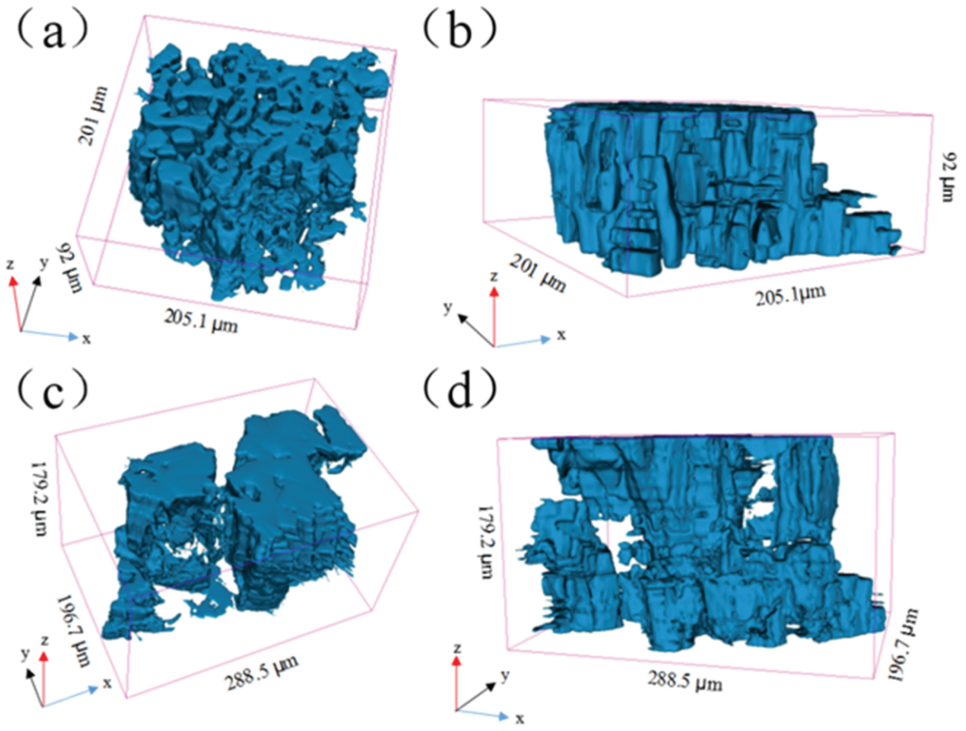

Figure 5: 3D microstructure of magnetite in vanadium-titanium sinter (a),(b) and in traditional sinter (c),(d).

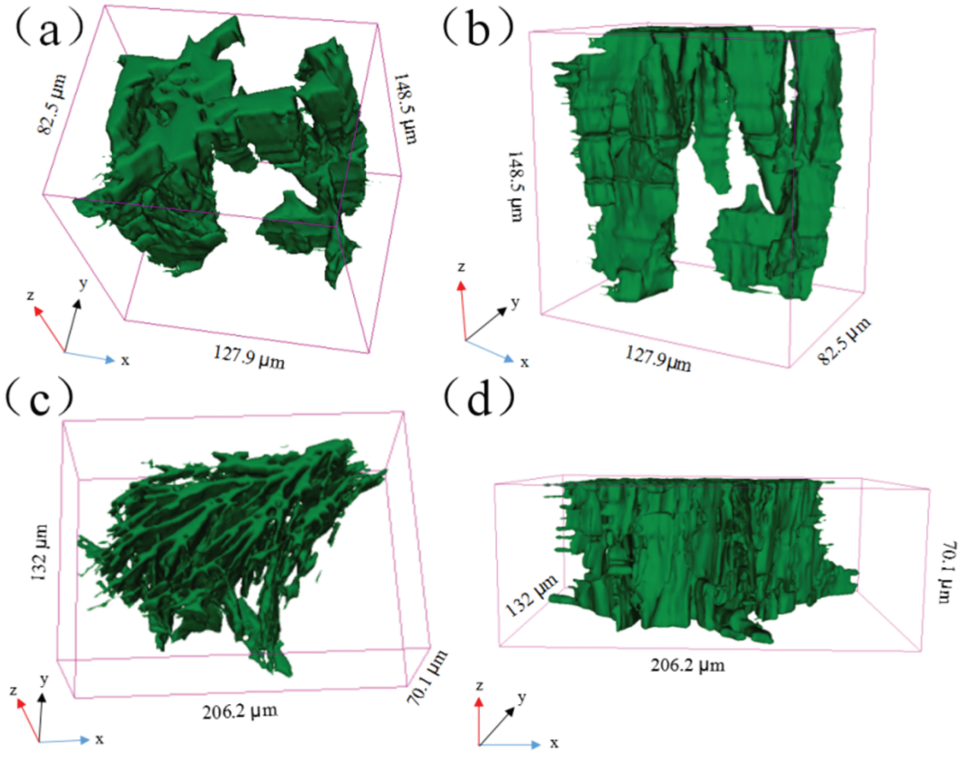

Figure 6: 3D microstructure of calcium ferrite in vanadium-titanium sinter (a), (b) and in traditional sinter (c), (d).

structure helps to improve the fracture toughness of the sinter.

Figure 5 is the 3D microstructure of magnetite in the two sinters. It can be observed that the size of the magnetite crystal in vanadium-titanium sinter is much smaller than that in traditional sinter, whereas the magnetite particles in vanadium-titanium sinter connect with each other to form a large magnetite group. The magnetite crystals in vanadium-titanium sinter are mainly granular-like grains with a regular shape in the horizontal direction, but most grains are a fine strip when viewed from the longitudinal direction. This structure leads to the poor connection of the magnetite crystals in vanadium-titanium sinter; thus, these structures are easy to fracture. In contrast, the magnetite in traditional sinter is smooth and appears as a euhedral crystal, which may be caused by good crystallization conditions. The change in the longitudinal direction is clear; some grains gradually increase, and some grains gradually decrease and disappear. Because the temperature range of the precipitation of the mineral crystal is small, many plate-like crystals are not fully dissolved, leaving an uneven crystal size. However, these structures contribute to the formation of the interwoven structure and favor the improvement of sinter strength.

The 3D structure of calcium ferrite in vanadium-titanium sinter is shown in Figure 6 (a) and (b). The columnar-like calcium ferrite consists of several dendritic crystals with different sizes. Some single columnar structures even exist in isolation. The size of calcium ferrite changes clearly along the longitudinal direction. The interface of the columnar calcium ferrite is smooth. The morphology of calcium ferrite in traditional sinter is quite different from that in vanadium-titanium sinter, as shown in Figure 6 (c) and (d). The calcium ferrite matrix in the 3D image is sheet-like, and many acicular crystals grow along different directions. Therefore, this structure makes it difficult to develop cracks in the direction parallel to the phase interface, which prevents the crack propagation and improves the mineral's fracture resistance [12].

The 3D perspective images of silicate in the two sinters are shown in Figure 7. The silicate in vanadium-titanium sinter is an allotriomorphic crystal that is small in size. The particle-like silicate distributes randomly in the sinter, as shown in Figure 7**(a)**. However, the silicate in traditional sinter coexists with calcium ferrite and acts as the binding phase, as shown in Figure 7**(b)**; therefore, appropriate silicate content will benefit the sinter strength.

The 3D perspective images of pores in the two sinters are shown in Figure 8. The pores in the two sinters are significantly different. The vanadium-titanium sinter has several big pores with sizes above 150 μm and many small closed pores, while the pores in traditional sinter are needle-like and connect with each other to form a complicated pore group. The features of the pores in traditional sinter contribute to the diffusion of the reduction gas and result in its better reducibility.

Quantitative statistics of a single mineral

Panoramic images of the polished sinters were obtained using an optical digital microscope (DSX510). Subsequently, the images were obtained with the 3D Slicer software, and the pores and minerals were marked with different colors, as shown in Figure 9. Because the length of 100 μm in the actual sample corresponds to 108 pixels in the panoramic image, the areal proportion of different minerals in the sinter can be obtained through the statistical analysis of the pixel points of each mineral based on the function of the pixel statistics provided by the 3D slice software. The area fractions of the minerals in the two sinters are shown in Figure 10.

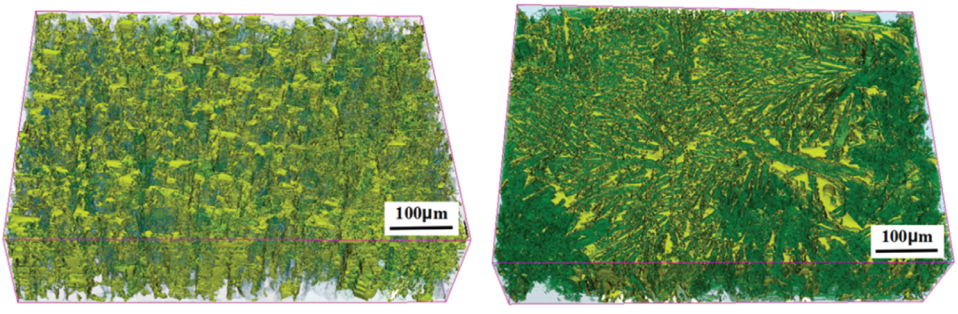

Figure 7: 3D perspective images of silicate in sinters. (a) Vanadium-titanium sinter; (b) Traditional sinter.

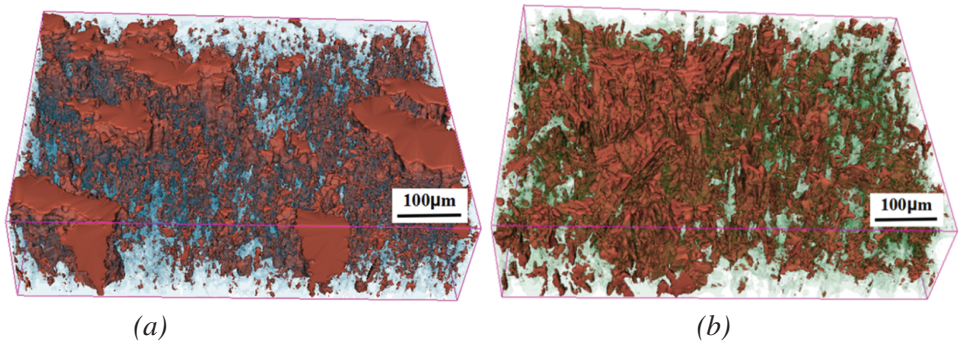

Figure 8: 3D perspective images of pore in sinters.

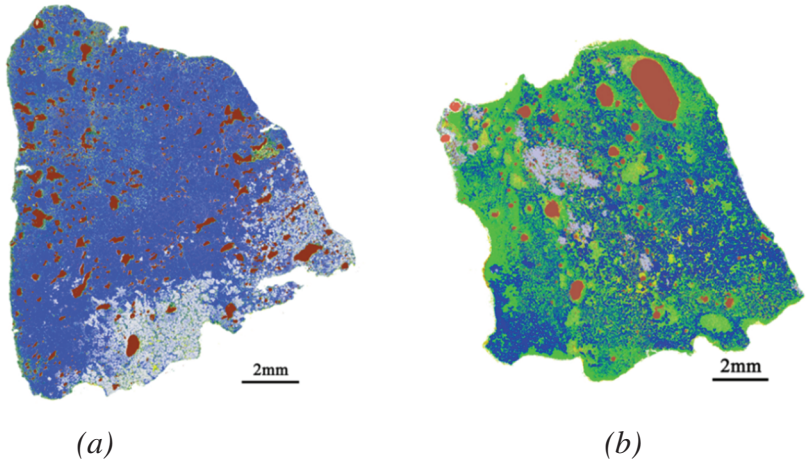

Figure 9: Threshold segmentation images of sinters. (a) Vanadium-titanium sinter; (b) Traditional sinter.

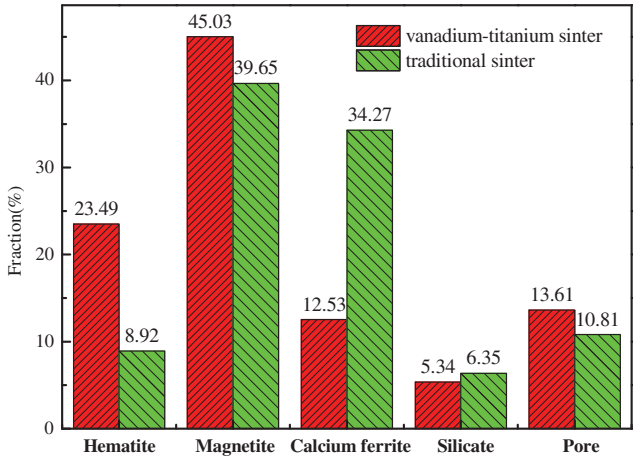

Figure 10: Calculated fraction of minerals in the two sinters.

From Figure 9 and Figure 10, the most prominent mineral in the two sinters is magnetite. The mineral content from highest to lowest in vanadium-titanium sinter is magnetite, hematite, calcium ferrite and silicate, and in traditional sinter, the order is magnetite, calcium ferrite, hematite and silicate. Through the above analysis on the 3D morphology and area fraction of minerals in the two sinters, it can be obtained that the mineral microstructure has a significant difference between vanadium-titanium sinter and traditional sinter, which results in their different metallurgical properties. A previous study revealed that the crystal transformation of hematite during reduction could lead to sinter degradation, and therefore, the higher hematite content in vanadium-titanium sinter resulted in its lower reduction degradation index. In addition, calcium ferrite has the best reduction ability. Therefore, the higher calcium ferrite content in traditional sinter results in its better reduction property.

Micromechanical properties of minerals

The metallurgical properties of a sinter are linked closely with the micromechanical properties of the minerals in

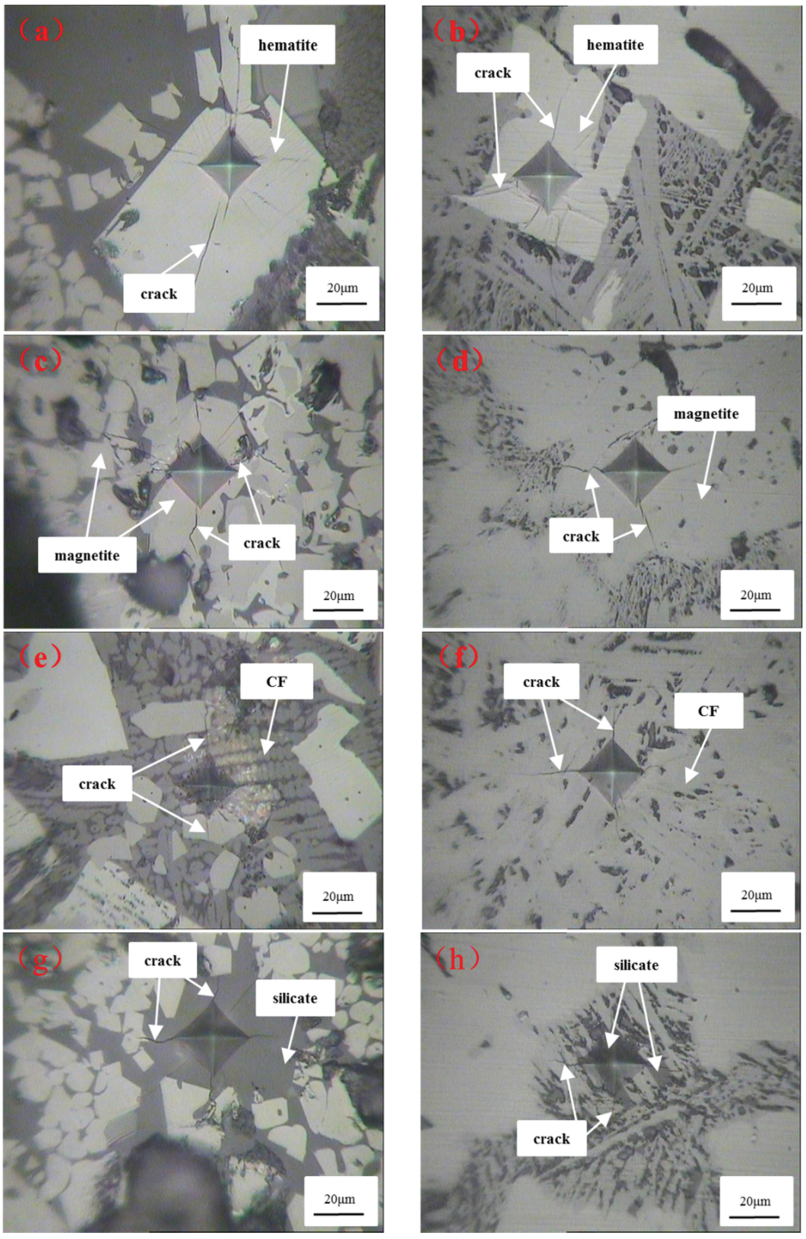

Figure 11: Indentations of different minerals in the two sinters. (a), (c), (e), and (g) represent the minerals in vanadium-titanium sinter; (b), (d), (f),and (h) represent the minerals in traditional sinter.

the sinter. The microhardness values of the minerals in the two sinters were tested by a Vickers hardness tester, and the fracture toughness value was calculated according to the size of the cracks. The indentations of different minerals in the sinter are shown in Figure 11. The micromechanical property indices are listed in Tables 3 and 4.

From Figure 11 (a) and (b), the area of indentation of hematite is large, and the size of the crack is approximately 50 μm in vanadium-titanium sinter. Furthermore, the indentation of hematite in traditional sinter is shallow, its crack size is shorter, and most cracks disappear at the crystal boundary. From Tables 3 and 4, it can be found that the average microhardness value (average H_V) of hematite in the two sinters is similar, while the average fracture toughness value (average K_{IC}) of hematite in traditional sinter is greater than that in vanadium-titanium sinter, indicating that the hematite in the two sinters has similar hardness, but the resistance to fracture of hematite in traditional sinter is better than that in vanadium-titanium sinter.

From Figure 11 (c) and (d), there are several short cracks that are approximately 12–25 μm around the indentation

Table 3: Indices of micromechanical properties of vanadium-titanium sinter.

Mineral	H_V/(Gg/m^2)	Average H_V/(Gg/m^2)	Average K_{IC}/(MN/m$^{3/2}$)
Hematite	937.4 ~ 993.7	963.5	1.25
Magnetite	644.8 ~ 716.9	686.5	0.93
Calcium ferrite	787.7 ~ 853.9	823.9	1.62
Silicate	590.4 ~ 682.2	608.9	0.55

Table 4: Indices of micromechanical properties of traditional sinter.

Mineral	H_V/(Gg/m^2)	Average H_V/(Gg/m^2)	Average K_{IC}/(MN/m$^{3/2}$)
Hematite	861.6 ~ 1055.2	961.1	1.36
Magnetite	737.7 ~ 808.9	756.2	1.13
Calcium ferrite	780.9 ~ 853.8	815.9	1.52
Silicate	625.7 ~ 716.9	548.2	0.75

of magnetite in the two sinters. The tested results of the micromechanical properties show that the average microhardness value and average fracture toughness value of magnetite in vanadium-titanium sinter are less than that in traditional sinter. Meanwhile, the cracks around the indentation of calcium ferrite in vanadium-titanium sinter are much shorter than those in traditional sinter, as shown in Figure 11 (e) and (f), and the tested results also show that the average microhardness value and average fracture toughness value of calcium ferrite in vanadium-titanium sinter are greater than those in traditional sinter, indicating better micromechanical properties of calcium ferrite in vanadium-titanium sinter.

For the indentation of silicate in the two sinters, as shown in Figure 11 (g) and (h), the number of cracks around the silicate indentation in the vanadium-titanium sinter is much greater than that in traditional sinter, which indicates that the silicate in vanadium-titanium sinter is more brittle and easier to fracture. This conclusion is confirmed by the average fracture toughness values (average K_{IC}) in Tables 3 and 4. However, form the tested results of the microhardness, silicate in vanadium-titanium sinter has better hardness. From the above analysis, it can be concluded that calcium ferrite has the greatest fracture toughness value and a very good strength. Therefore, some measures should be taken to increase the content of calcium ferrite in vanadium-titanium sinter, such as adjusting the alkalinity and sintering temperature, and so on.

The average microhardness value of the minerals in the two sinters from highest to lowest is in the order of hematite, calcium ferrite, magnetite and silicate, while the decrease order of average fracture toughness is in the order of calcium ferrite, hematite, magnetite and silicate. To quantitatively evaluate the mechanical properties of the sinter, the comprehensive hardness value and the comprehensive fracture toughness value were defined based on the area fraction of the minerals and the indices of the micromechanical properties. The calculated equation is as follows:

$$H_{VT} = S_1 H_{V1} + S_2 H_{V2} + \cdots + S_n H_{Vn} \tag{3}$$

$$K_{ICT} = S_1 K_{IC1} + S_2 K_{IC2} + \cdots + S_n K_{ICn} \tag{4}$$

where H_{VT} is the comprehensive hardness value of the sinter, Gg/m^2; S_1, S_2 and S_n are the area fraction of the different minerals, %; H_{V1}, H_{V2} and H_{Vn} are the microhardness value of different mineral, G g/m^2; K_{ICT} is the comprehensive fracture toughness value of sinter, MN/m$^{3/2}$; K_{IC1}, K_{IC2} and K_{ICn} are the fracture toughness values of different minerals, MN/m$^{3/2}$. The comprehensive hardness value and fracture toughness value were calculated based on the above experimental data, as shown in Table 5.

From the calculated results in Table 5, the comprehensive hardness value and comprehensive fracture toughness value of the vanadium-titanium sinter are 659.23 G g/m^2 and 0.96 MN/m$^{3/2}$, which are both less than those of traditional sinter. Moreover, the decreased reduction degradation index and tumbler index of vanadium-titanium sinter perfectly match its lower comprehensive hardness value and comprehensive fracture toughness. Therefore, a good micromechanical property of the sinter should also be pursued in practice. Further

Table 5: Comprehensive hardness value and fracture toughness value of sinter.

Sample	H_{VT}/(Gg/m^2)	K_{ICT}/(MN/m$^{3/2}$)	$RDI_{-3.15}$/%	TI/%
Vanadium-titanium sinter	659.23	0.96	62.46	68.19
Traditional sinter	699.98	1.14	34.15	79.25

study on the quantity relationship between the comprehensive hardness value as well as the comprehensive fracture toughness of sinter and its metallurgical properties should be explored in the future.

Conclusions

The 3D images of vanadium-titanium sinter and traditional sinter were reconstructed in this study, and the 3D microstructure and micromechanical properties of the minerals were investigated. Some conclusions were obtained as follows:

(1) More information about the minerals in sinter can be obtained from the reconstructed 3D images. The hematite and magnetite crystals in vanadium-titanium sinter grow along the longitudinal axis direction and play a role as the scaffold in the sinter. Some small minerals, such as calcium ferrite and silicate, are wrapped by the large hematite or magnetite. However, the primary minerals in a traditional sinter are calcium ferrite and magnetite, and they grow along different directions.

(2) The morphology of the hematite crystal in vanadium-titanium sinter is less irregular than that in traditional sinter. The size of the magnetite crystal in vanadium-titanium sinter is much smaller than that in traditional sinter, but these small magnetite particles connect with each other to form a large magnetite group. The calcium ferrite in vanadium-titanium sinter is columnar-like compared to the needle-like character in traditional sinter. The area fraction of a mineral from highest to lowest in vanadium-titanium sinter is magnetite, hematite, calcium ferrite and silicate, and the value is 45.03%, 23.49%, 13.61%, 12.53% and 5.34%, respectively. Whereas the decreasing order of the mineral content in traditional sinter is magnetite, calcium ferrite, hematite and silicate, whose value is 39.65%, 34.27%, 10.81%, 8.92% and 6.35%, respectively.

(3) The average microhardness value of the minerals in the two sinters in decreasing order is hematite, calcium ferrite, magnetite and silicate, while the average fracture toughness value from highest to lowest is calcium ferrite, hematite, magnetite and silicate. The high content of calcium ferrite is good for the metallurgical properties of vanadium-titanium sinter. Therefore, some measures contributing to the increase in calcium ferrite should be taken in practice. Moreover, the lower reduction degradation and tumbler indices of vanadium-titanium sinter perfectly match its lower comprehensive hardness value and comprehensive fracture toughness compared to traditional sinter. Therefore, a good micromechanical property of sinter should also be pursued in practice.

Acknowledgements: The authors acknowledge the financial support for the National Natural Science Foundation of China (51474164, U201760101, 51704216) and the China Postdoctoral Science Foundation (2016M602378).

References

[1] V. Shatokha, I. Korobeynikov, E. Maire and J. Adrien, Ironmak. Steelmak., 36 (2009) 416–420.
[2] X. Fan, Z. Ji, M. Gan, X. Chen, Q. Li and T. Jiang, Ironmak. Steelmak., 43 (2016) 5–10.
[3] M. Zhou, T. Jiang, S. Yang, Y. Wang, L. Zhang and X. Xue, Iron. Steel., 50 (2015) 10–15.
[4] X.H. Fan, Z.H. Zhao, X.L. Chen, M. Gan and Y. Wang, J. Central South Univ., 42 (2011) 2893–2897.
[5] X. Lv, C. Bai, G. Qiu, M. Hu and S. Zhang, ISIJ Int., 48 (2008) 186–193.
[6] X. Lv, C. Bai, G. Qiu, S. Zhang and M. Hu, ISIJ Int., 49 (2009) 709–718.
[7] V. Shatokha, Iron. Steel., 37 (2010) 313–319.
[8] E. Kasai, W.J. Rankin, R.R. Lovel and Y. Omori, ISIJ Int., 29 (1989) 635–641.
[9] S. Kasama, T. Inazumi and T. Nakayasu, ISIJ Int., 34 (1994) 562–569.
[10] M. Nakano, T. Kawaguchi, S. Kasama, T. Inazumi, J. Torii and T. Nakano, ISIJ Int., 37 (1997) 339–344.
[11] R. Wang, Sinter Pellet, 20 (1995) 9–13.
[12] S. Wang and X. Bi, WISCO Technol., 47 (2009) 19–22.
[13] N. Sakamoto, H. Fukuyo, Y. Iwata and T. Miyashita. Proceedings of Symposium on Burden Design for the Blast Furnace, McMaster University, Canada, (1984) 137–151.
[14] Z.W. Ying, L.X. Xu, M.F. Jiang and Y.S. Shen, J. Iron. Steel Res. Int., 18 (2006) 55–58.

[15] I. Shigaki, M. Sawada, K. Yoshioka and T. Takahashi, Tetsu-to-Hagane, 71 (1985) 1880–1887.
[16] C.E. Loo, K.T. Wan and V.R. Howes, Iron. Steel., 15 (1988) 279–285.
[17] L. Cheng, K. Wu, X. Wan, H. Zhang and J. Iron, Steel Res. Int., 21 (2014) 964–968.
[18] K. Wu, Acta Metalluergical Since, 41 (2005) 1237–1242.
[19] B. Yang, Transa Nonferrous Met. Soc. China, 24 (2014) 833–838.
[20] N. Chawla, R.S. Sidhu and V.V. Ganesh, Acta Mater., 54 (2006) 1541–1548.
[21] W. Wang, M. Deng, R. Xu, W. Xu, O. Zelin, X. Huang and Z. Xue, J. Iron. Steel Res. Int., 24 (2017) 998–1006.
[22] J. Gong and Z. Guan, Int. J. Inorg. Mater., 17 (2002) 96–104.
[23] B. Liu, Y. Fan, J. Zhang and J. Pan, Chin J. Nonferrous Met., 11 (2001) 810–814.
[24] J. Wang, D. Ma, M. Bai, Y. Huang and L. Sun, J. Mat. Eng., 43 (2015) 81–88.